

Mechanisms of convection-induced modulation of passive tracer interhemispheric transport interannual variability

Benjamin R. Lintner

Berkeley Atmospheric Sciences Center and Department of Geography, University of California, Berkeley, California, USA

Alice B. Gilliland¹

Atmospheric Sciences Modeling Division, Air Resources Laboratory, NOAA, Research Triangle Park, North Carolina, USA

Inez Y. Fung

Berkeley Atmospheric Sciences Center and Department of Earth and Planetary Sciences, University of California, Berkeley, California, USA

Received 31 October 2003; revised 23 March 2004; accepted 9 April 2004; published 1 July 2004.

[1] Interannual variations of tropical convection impact atmospheric circulation and influence year-to-year variations of the transport of trace constituents in the troposphere. This study examines how two modes of convective variability, anomalous intensification and meridional displacement of centers of tropical convection, impact interhemispheric transport (IHT) interannual variability. Two modeling frameworks are employed, an atmospheric general circulation model (AGCM) and a chemical transport model (CTM) forced with a realistic, interannually varying circulation field, to investigate the zonally averaged and regional-scale influences of the modes of convective variability on passive tracer IHT. Both convective modes are found to modulate IHT interannual variability. While convective displacement appears to be the more quantitatively significant mode within the AGCM framework, anomalous convective intensity and displacement are of equal importance in the CTM framework. The results suggest that the modeling of atmospheric tracer transport interannual variability requires accurate representation of multiple aspects of convective variability. *INDEX TERMS*: 0368 Atmospheric Composition and Structure: Troposphere—constituent transport and chemistry; 1620 Global Change: Climate dynamics (3309); *KEYWORDS*: interhemispheric transport, interannual variability, convection, tracer transport

Citation: Lintner, B. R., A. B. Gilliland, and I. Y. Fung (2004), Mechanisms of convection-induced modulation of passive tracer interhemispheric transport interannual variability, *J. Geophys. Res.*, 109, D13102, doi:10.1029/2003JD004306.

1. Introduction

[2] Atmospheric trace constituents with Northern Hemisphere sources exhibit steep gradients across the equator [Plumb and Mahlman, 1987; Plumb and McConalogue, 1988]. Interhemispheric gradients associated with passive tracers may provide information about mixing characteristics in the equatorial region where traditional atmospheric circulation statistics are relatively symmetric. That is, the steepness of the interhemispheric gradient is related to the relative amount of mixing between the hemispheres. A number of mechanisms have been proposed as generators of interhemispheric transport (IHT) in the climatological mean sense. Among the most significant generators of IHT are convective mixing/upper level divergent outflow

[Prather *et al.*, 1987; Hartley and Black, 1995], Hadley circulation seasonality [Bowman and Cohen, 1997], cross-equatorial monsoons [Wang and Shallcross, 2000], and lateral eddy mixing and wave breaking [Staudt *et al.*, 2001].

[3] Analyses of the year-to-year variations of IHT have been relatively uncommon, in part because IHT interannual fluctuations are small compared to either the time mean or seasonal variations of IHT. Past studies of observed atmospheric chemical constituents (e.g., CFC-11 and SF₆) from the NOAA CMDL and ALE/GAGE networks have suggested potential interannual variations of IHT [Steele *et al.*, 1992; Elkins *et al.*, 1993; Cunnold *et al.*, 1994; Dlugokencky *et al.*, 1994; Hartley and Black, 1995]. However, observed tracer data have been unable to substantiate global IHT interannual variations definitively because of the short duration (typically <20 years) of the observations, the lack of consistent calibration of the measurements, and the sparse spatial coverage of the observational network, particularly in the vertical. The only direct way to quantify IHT rates is to use

¹On assignment to National Exposure Research Laboratory, U.S. Environmental Protection Agency, Research Triangle Park, North Carolina, USA.

models to account for the total atmospheric mass budget, but the use of models adds uncertainty to the analysis.

[4] Model-derived IHT is the result of circulation physics in the model. Thus, while intermodel differences, e.g., convective mixing or planetary boundary layer parameterization, impart much uncertainty to the estimates of model-derived IHT, the same intermodel differences may illustrate the sensitivity of IHT to different transport and mixing mechanisms. For example, *Gilliland and Hartley* [1998] found that annual mean rates of IHT differed by approximately 35% between two versions of the NCAR Community Climate Model (CCM2 and CCM3) with differing convective parameterization; the model version with more intense vertical convective mass flux produced stronger IHT. Results from the International Geosphere-Biosphere Programme Transport Intercomparison Project (TransCom) [Denning et al., 1999; Gurney et al., 2003], for which over 10 global atmospheric circulation/transport models simulated tracer distributions for the same source emissions, further highlight the sensitivity of simulated IHT to model framework, as the models produced a broad range for the characteristic timescale of IHT (i.e., 0.55–1.26 years). In spite of the drawbacks inherent in both the observational and modeling approaches, analyses of the interannual variability of IHT offer some valuable insights into the mechanistic interpretation of interhemispheric transport. A better understanding of the mechanisms driving IHT variations at interannual timescales may ultimately contribute to improving and refining model processes involved in the simulation of IHT.

[5] Of all potential IHT mechanisms, convective mixing has garnered particular attention as a generator of IHT. For example, *Hartley and Black* [1995] used NCAR CCM2 to demonstrate that upper level outflow associated with regions of deep convection provides an important pathway of tracer mixing between the hemispheres, at least in a climatological sense. More recently, in a study of the impact of a doubled CO₂ climate on tracer distributions, *Rind et al.* [2001] noted that a simulated 5% reduction in the strength of the Hadley circulation induced by CO₂ doubling increases the timescale of IHT by a similar percentage. However, the analysis of *Gilliland* [1997] suggests little relationship between the intensity or areal extent of deep convection and interannual changes in IHT as simulated by NCAR CCM3. Moreover, while noting the potential importance of convective intensity in explaining intermodel variations of exchange time, *Rind and Lerner* [1996] emphasized that the meridional position of convective activity may be more directly responsible for establishing intermodel differences in interhemispheric mixing. *Gilliland* [1997], in fact, argued that interannual changes in passive tracer IHT may be related to anomalous meridional displacements of tropical convection, at least during the ENSO events of the late 1980s.

[6] Previous studies suggest two aspects of convective variability that may modulate IHT at interannual timescales. One possible means of convective influence, anomalous variations in the intensity of convection, is supported by various model intercomparison studies [*Gilliland and Hartley*, 1998; *Denning et al.*, 1999] that demonstrate a relationship between the strength of convection and the amount of upper level tracer outflow. Generalizing the

intercomparison results to interannual variations suggests that anomalous strengthening of convection may generate more surface to upper level tracer mass transport and “faster” interhemispheric mixing. Another way that convection may modulate IHT interannual variability is through anomalous displacement of convective activity, since the meridional position of convection influences where (and ultimately how) air masses mix between the hemispheres. In the present analysis, the potential influences of both of these modes of convective variability on tracer transport are investigated. Although the two aspects of convective variability are treated separately, it should be noted that both convective location and strength variations may occur concurrently, as for example during ENSO events [*Janicot*, 1997; *Chiang et al.*, 2000; *Giannini et al.*, 2001].

2. Methodology

2.1. Models

[7] The principal model used in this study is the atmospheric general circulation model (AGCM) of the Goddard Institute for Space Studies (GISS) [*Hansen et al.*, 1997], with minor modifications made at the University of California, Berkeley (UCB) to incorporate tracer transport. The GISS-UCB AGCM solves the primitive equations on a grid of coarse horizontal resolution (4° × 5°) and nine unevenly spaced sigma levels in the vertical. By design, seven of the vertical levels are located below the tropopause. Parameterizations of all relevant physical processes, including radiative transfer, moist and dry convection, and planetary boundary layer processes, are included. The convective parameterization scheme implemented in the GISS-UCB AGCM is described by *Del Genio and Yao* [1988, 1993]. The amount of convective mass flux is obtained via a closure assumption that restores the cloud base to neutral buoyancy relative to the next highest layer. Tracers are advected using the slopes scheme [*Russell and Lerner*, 1981], and turbulent mixing of tracers in the vertical follows dry and moist convection of temperature and moisture. Simulations of atmospheric circulation interannual variability by the GISS AGCM have been shown to be realistic [*Chan and Evans*, 2002; *Vuille et al.*, 2003].

[8] The GISS-UCB AGCM (or hereinafter “AGCM”) is forced interannually by boundary conditions in sea surface temperature and sea ice cover and by varying atmospheric composition (CO₂, tropospheric O₃, and volcanic aerosols) for the period January 1979 to December 1994. The sea surface temperature and sea ice cover boundary conditions are identical to those used by the Atmospheric Model Intercomparison Project [*Gates et al.*, 1999], and the atmospheric composition changes are similar to those described by *Hansen et al.* [1997]. An ensemble of five AGCM integrations with identical forcing but different initial conditions is discussed here. The initial conditions for the five ensemble members are the atmospheric states of five randomly chosen December 31st's of a 15-year control run in which climatological boundary condition forcing is applied, and atmospheric composition is fixed. A passive tracer with a time-invariant, predominately Northern Hemisphere, source emission function resembling the pattern of sulfur hexafluoride (SF₆) emissions is modeled “on-line” such that circulation variability

directly affects tracer transport and distribution in the atmosphere.

[9] The second model utilized in this study is the Model of Atmospheric Transport and Chemistry (MATCH) [Mahowald *et al.*, 1997; Rasch *et al.*, 1997; Rasch and Lawrence, 1998] forced with a realistic reanalysis circulation. Dargaville *et al.* [2003] simulated the interannual distribution of a passive tracer with a time-invariant SF₆ source in MATCH using the circulation field from the NCEP/NCAR 40-Year Reanalysis [Kalnay *et al.*, 1996]. This reanalysis circulation field represents a “best guess” approximation to the state of the atmosphere over the simulation period. A total of 29 years of simulation was archived; the 28-year period spanning January 1971 to December 1998 is analyzed here. The NCEP/MATCH (hereinafter “CTM”) exchange time variability is compared to monthly mean convection (precipitation rate) and wind data obtained from the NCEP/NCAR website (available at <http://ingrid.ldeo.columbia.edu/SOURCES/NOAA/NCEP-NCAR/CDAS-1/MONTHLY/>).

2.2. Interhemispheric Transport and Convection Measures

[10] The interhemispheric exchange time (τ), a commonly used measure of IHT, is obtained via a two-box model framework applied to the three-dimensional tracer mass field. The two-box model consists of a set of two first-order, coupled differential equations governing the time evolution of tracer mass within each hemisphere, namely:

$$\begin{aligned} \frac{\partial M_n}{\partial t} &= S_n - \frac{(M_n - M_s)}{\tau} \\ \frac{\partial M_s}{\partial t} &= S_s + \frac{(M_n - M_s)}{\tau}. \end{aligned} \quad (1)$$

Here M_n and M_s are the total vertically and horizontally integrated masses of tracer (in kg) in the Northern and Southern Hemispheres, respectively; S_n and S_s are the Northern and Southern Hemisphere integrated source emissions (in kg/year); and τ is in years. The gradient terms on the right-hand side of equations (1) represent the net flux of tracer mass from the Northern to the Southern Hemisphere. As constructed, both atmospheric sources and sinks of tracers are implicitly included in the source emissions, and no chemical loss is assumed because of the assumed chemical inactivity of the tracer. Equations (1) may be combined and inverted to obtain an expression for the exchange time as a function of the tracer mass and source emission gradients:

$$\tau = \frac{2(M_n - M_s)}{S_n - S_s - \frac{\partial(M_n - M_s)}{\partial t}}. \quad (2)$$

Unless otherwise stated, all mass and source integrals are computed by assuming that the hemispheric partition is coincident at all pressure levels and longitudes with the geodetic equator. Vertical integrals cover the entire vertical domain in each model.

[11] For stationary sources with emissions localized to the Northern Hemisphere, the exchange time may be interpreted as a “lag-response” for the hemispheric tracer

Table 1. Regional ITCZs^a

Region	Abbreviation	Interval
Africa	AFR	10°E–40°E
Indian Ocean/South Asia	IND	60°E–100°E
Western Pacific	WPA	110°E–150°E
Central Pacific	CPA	160°E–160°W
Eastern Pacific	EPA	140°W–110°W
South America	SAM	75°W–45°W
Atlantic Ocean	ATL	40°W–10°W
Global	GLO	180°W–175°E

^aFollowing Waliser and Gautier [1993].

masses [Bowman and Cohen, 1997]. That is, τ corresponds to the time required for the mass of tracer in the Southern Hemisphere (the nonsource hemisphere) to achieve, at a time t , the mass of tracer achieved in the Northern Hemisphere (the source hemisphere) at an earlier time $t - \tau$. It should be mentioned that the characteristics of τ , such as its mean value or seasonality, may depend on other factors besides the strength of interhemispheric mixing, including the timescale for mixing between the source regions and the tropics and the vertical profile of the tracer distribution.

[12] The convective intensity and displacement measures are derived from the precipitation rate field. For each longitude ϕ and at each month t , both the maximum value of the precipitation rate between 15°S and 15°N, $ppt_{\max}(\phi, t)$, and the latitude of occurrence of the maximum value, $\lambda_{\max}(\phi, t)$, are identified. Convective intensity or strength (*STR*) is defined as the average precipitation rate maximum over the interval between bounding longitudes ϕ_1 and ϕ_2 :

$$STR(t) = \frac{\int_{\phi_1}^{\phi_2} ppt_{\max}(\phi, t) d\phi}{\int_{\phi_1}^{\phi_2} d\phi}. \quad (3)$$

Convective displacement or location (*LOC*) is defined as the longitudinal interval average of the latitude of maximum precipitation rate occurrence weighted with respect to the precipitation rate maxima at each longitude:

$$LOC(t) = \frac{\int_{\phi_1}^{\phi_2} \lambda_{\max}(\phi, t) ppt_{\max}(\phi, t) d\phi}{\int_{\phi_1}^{\phi_2} ppt_{\max}(\phi, t) d\phi}. \quad (4)$$

This weighting procedure biases the estimate of the interval-averaged displacement toward regions with the largest precipitation rates. Both global and regional longitudinal intervals (summarized in Table 1) are considered, with regional intervals corresponding to those defined in the ITCZ climatology study of Waliser and Gautier [1993].

2.3. Notation and Analysis Methods

[13] In this study both regressions and composites are computed. Consider two N-element time series x and y with means \bar{x} and \bar{y} . Anomalies of x and y are defined as $x' = x - \bar{x}$ and $y' = y - \bar{y}$. Unless otherwise stated, anomalies are calculated with respect to monthly mean climatologies computed over the entire length of the time series. The linear-least

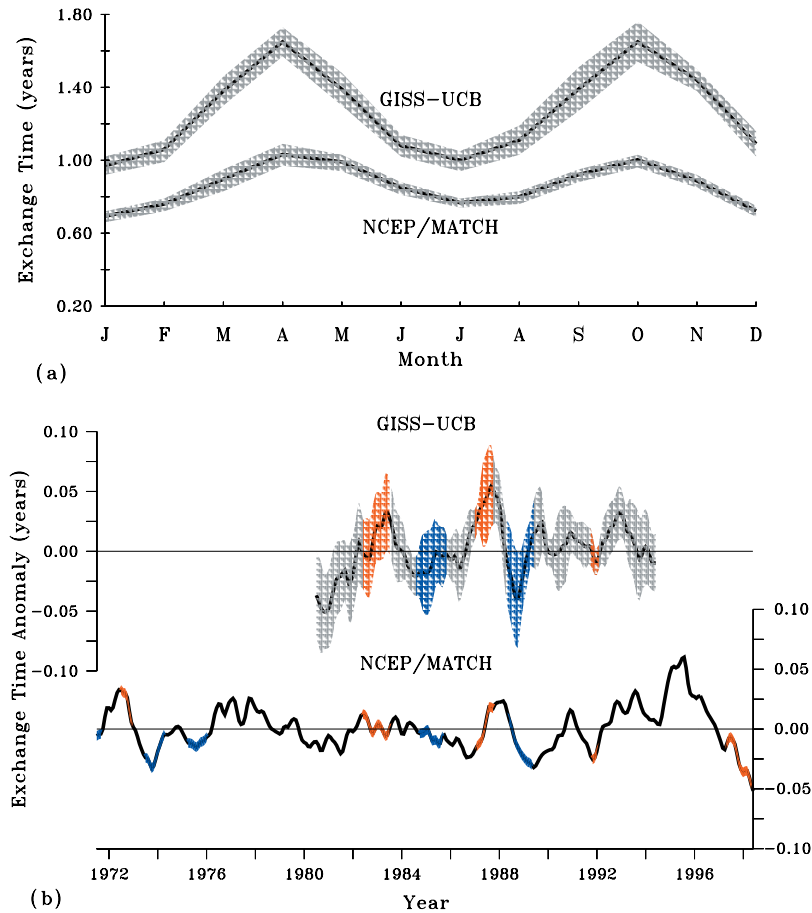


Figure 1. GISS-UCB AGCM and NCEP/MATCH exchange time (a) seasonal cycles and (b) interannual variations. In Figure 1a the error envelopes represent year-to-year standard deviations of the monthly values. (The error envelopes are aggregated over the entire ensemble for the AGCM.) In Figure 1b the anomalies illustrated are 12-point running means of deseasonalized monthly exchange times for the AGCM (top curve) and CTM (bottom curve), and red and blue shading denotes El Niño and La Niña phase conditions, respectively. The error envelope of the top curve represents the standard deviation of the ensemble mean.

squares regression of y' onto x' , denoted as y^* , is given by $y^* = \frac{\sigma_y}{\sigma_x} r(x', y') x'$, where $r(x', y')$ is the correlation coefficient of x' and y' , and σ_x and σ_y are the standard deviations of x and y . For a “1 sigma” anomaly in x' , the corresponding linear regressive anomaly estimate y^* is $\sigma_y r(x', y')$.

[14] Composites of a time series or field y computed with respect to a time series x' are constructed as follows. Elements of x' are divided into subsets according to a selection criterion; in this analysis, three subsets (or phases) are identified, namely, $x' \geq \sigma_x$, $x' \leq -\sigma_x$, and $-\sigma_x < x' < \sigma_x$. Separate phase averages of y are computed with respect to the positive and negative phases of x' :

$$y_{x' \geq \sigma_x} = \frac{\sum_{i=1}^N y'_i \Theta(x'_i - \sigma_x)}{\sum_{i=1}^N \Theta(x'_i - \sigma_x)} \quad (5)$$

$$y_{x' \leq -\sigma_x} = \frac{\sum_{i=1}^N y'_i \Theta(\sigma_x - x'_i)}{\sum_{i=1}^N \Theta(\sigma_x - x'_i)},$$

where

$$\Theta(x - x_0) = \begin{cases} 1, & x \geq x_0 \\ 0, & x < x_0 \end{cases}$$

is the Heaviside function. The composite difference, $\Delta y_{x'}$, is defined as $y_{x' \geq \sigma_x} - y_{x' \leq -\sigma_x}$. Standard deviations are computed separately for each phase average. For all AGCM calculations an ensemble mean standard deviation is obtained by aggregating the standard deviations of the five ensemble members.

3. Results

3.1. Exchange Time Seasonal Cycle and Interannual Variations

[15] Monthly mean exchange times calculated for the AGCM and CTM using equation (2). The seasonal cycles of the exchange time are illustrated in Figure 1a. The time mean values of annually averaged τ are 1.27 years and 0.86 years for the AGCM and CTM, respectively. It should be noted that the mean exchange time in the AGCM runs is large (indicative of slow mean IHT) compared to either the CTM τ or the range of exchange times noted in the TransCom intercomparison [Denning *et al.*, 1999]. However, the AGCM exchange time exhibits qualitatively similar seasonality to other model exchange times as well as the CTM exchange time, i.e., fast transport during solstice seasons

and slow transport during transition seasons with seasonal variations on the order of $\pm 30\%$ of the time mean [Levin and Hesshaimer, 1996; Gilliland and Hartley, 1998]. Such seasonality is consistent with variations in the intensity of the cross-equatorial component of the Hadley circulation [Oort and Yienger, 1996; Dima and Wallace, 2003].

[16] Figure 1b illustrates 12-point running means of deseasonalized, monthly mean exchange time anomalies (τ') for the AGCM (upper time series) and the CTM (lower time series). Here, each model's time mean, annually averaged exchange time has been removed. Additionally, the AGCM time series represents the ensemble mean of the 5 ensemble members, with the stippling denoting the 1σ level of the ensemble mean. It can be seen that interannual variations of both the AGCM and CTM τ' are small compared to either the time mean exchange time or its seasonal excursions, with a characteristic range between positive and negative anomalies of order 0.15 years in the AGCM and 0.07 years in the CTM simulation. Although some attenuation of the CTM τ' interannual variations relative to those of the AGCM may be expected based on the lower mean exchange time of the former, the relative level of interannual variability appears to be lower in the CTM than in the AGCM. That is, the ratio of the characteristic interannual variations to the time mean is smaller (~ 0.08) in the CTM than in the AGCM (~ 0.12).

[17] Finally, a preferred phase relationship between the exchange time variations and ENSO is evident in the AGCM exchange times, with “slower” (“faster”) IHT associated with El Niño (La Niña) conditions. (Red shading in Figure 1b represents El Niño years and blue shading La Niña years.) Such a phase relationship is in agreement with other studies based on networks of long-lived tracers such as CH_3CCl_3 [Prinn et al., 1992, 1995]. However, the spread of anomalies among the AGCM ensemble members is nonnegligible, implying a role for model-generated internal variability (such as land surface-circulation feedbacks) as a source of IHT anomalies. The ENSO-IHT phase relationship is more variable and less conclusive in the CTM simulation. Indeed, not all of the CTM τ' excursions coincident with sizeable ENSO events are consistent with the “slow IHT-El Niño” relationship: the El Niños of 1991–1992 and 1997–1998, for example, are characterized by anomalously fast IHT.

3.2. Connections Between IHT and Circulation

[18] Motivation for the present study is provided in Figure 2, which shows the relationships between τ' and anomalies of zonal mean 1000 mbar meridional wind and precipitation rate. The shading displayed in these figures represents estimates of anomalies of 1000 mbar meridional wind (i.e., v_{1000}^*) and precipitation rate (i.e., ppt^*) that are associated with τ' as obtained by linear regression of the field anomalies, v_{1000}' and ppt' , onto τ' . That is, v_{1000}^* (ppt^*) represents the portion of v_{1000}' (ppt') that covaries with τ' . Note that v_{1000}^* and ppt^* are normalized such that they correspond to a $+1\sigma$ deviation of monthly τ' , and only those estimates significant at or greater than the 95% (90%) level according to a Two-Tailed Student's t-Test are illustrated for the AGCM (CTM). For comparison, the monthly zonal mean climatologies of v_{1000} and ppt (line contours) are also illustrated.

[19] The most prominent feature of v_{1000}^* (AGCM, Figure 2a; and CTM, Figure 2c; filled contours) is the sign reversal near the equator between the winter and summer seasons, with significant anomalies occurring close to the latitude of convergence of northerly and southerly winds. That is, anomalously slow rates of IHT ($\tau' > 0$) are associated with v_{1000}' that directionally oppose the climatological Hadley circulation, i.e., anomalous surface southerlies near 10°S during December-January-February (DJF) or anomalous surface northerlies near 10°N during June-July-August (JJA). Moreover, the weak relationship between v_{1000}' and τ' during the winter-summer and summer-winter transitions is consistent with the lack of a strong cross-equatorial component of the Hadley circulation during these periods.

[20] The spatiotemporal features of v_{1000}^* are in qualitative agreement with the meridional distribution of ppt^* (AGCM, Figure 2b; and CTM, Figure 2d; filled contours). For $\tau' > 0$ conditions during DJF, for example, the development of both an anomalous southerly flow ($v_{1000}' > 0$) just to the south of the equator is associated with a northward shift of convection. As a consequence, a meridional convective dipole is evident, with anomalously strong (weak) convection to the north (south) of the equator. Analogous to the seasonal behavior of v_{1000}^* , ppt^* reverses sign between DJF and JJA, with the center of the dipole pattern shifted northward by $\sim 5^\circ$ latitude. The results presented thus far show that both convective location and strength variations may modulate IHT: a meridional shift in convection is suggested by the dipolar distribution of convection anomalies, although variations in convective intensity along the ITCZ (especially in Northern Hemisphere summer) are also present. The relative contributions of convective displacement and intensity variations are analyzed below.

3.3. Relationship of IHT to Convective Displacement and Intensity

[21] To address the roles of convective location and strength variations in modulating IHT, we first present time series of zonally averaged ITCZ location (LOC) and strength (STR) for both the AGCM and CTM (Figure 3). Here, 12-point running means of each mode of convective variability are illustrated, with blue and red shading denoting “fast” and “slow” IHT conditions in each model. Also, for the AGCM results, envelopes denoting the 1σ level of the ensemble means of LOC and STR are included.

[22] Several features of the LOC (Figure 3a) and STR (Figure 3b) time series are noteworthy. First, some coupling is evident between the strength and location of convection, with anomalously strong convective conditions occurring with anomalous southward displacements of the ITCZ. These coordinated changes likely arise from the modulation of tropical convection by ENSO. Also, intercomparison of the AGCM and CTM variability reveals some qualitative agreement in the temporal behavior of convective displacement and intensity anomalies of both models. For example, a prominent southward shift of convection in 1983–1984 is seen in both the AGCM (Figure 3a, top curve) and CTM (Figure 3a, bottom curve), as is a peak in convective intensity in the late

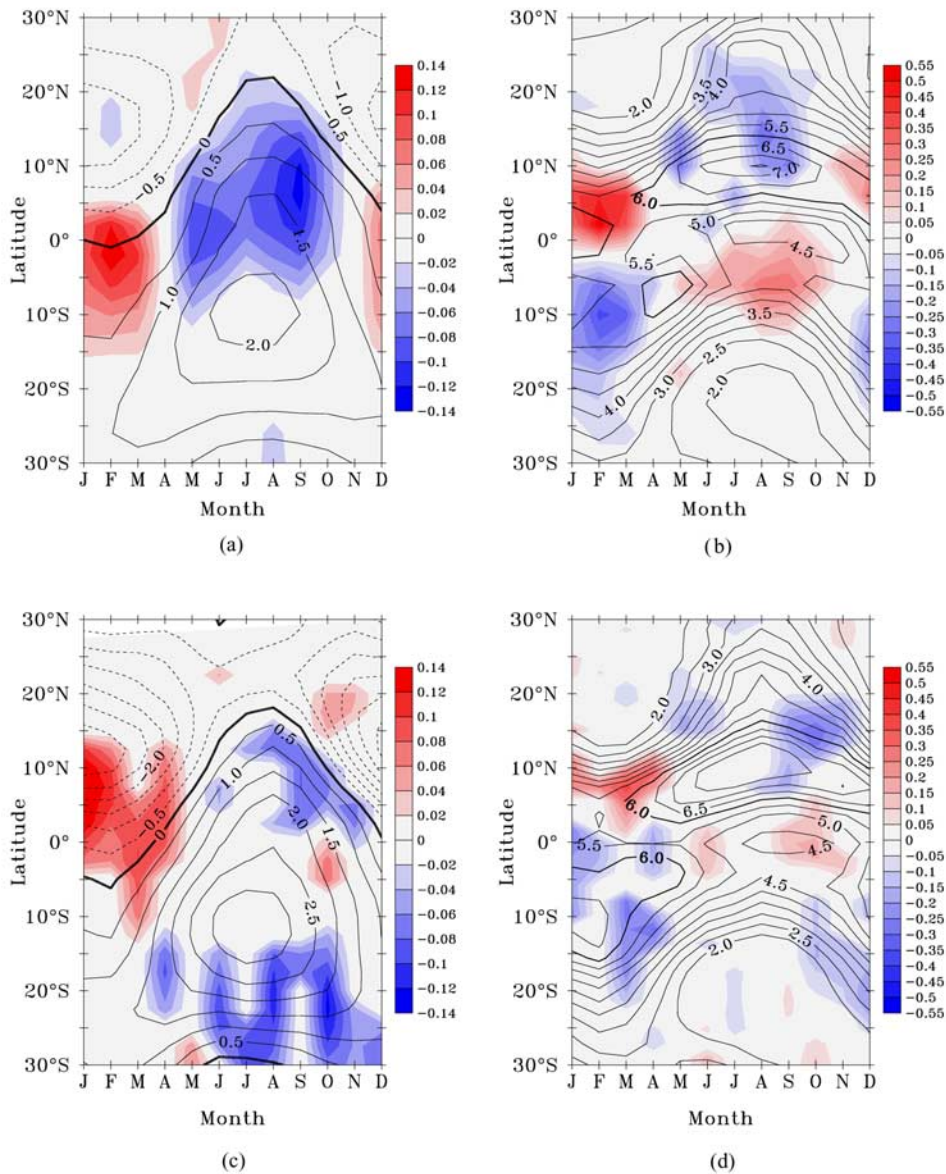


Figure 2. Relationship between anomalies of exchange time (τ') and zonal mean meridional wind at 1000 mbar (v'_{1000}) and precipitation rate (ppt') in the (a and b) AGCM and (c and d) CTM. Line contours represent the zonal mean climatology of each field (i.e., \bar{v}_{1000} in Figures 2a and 2c, and \bar{ppt} in Figures 2b and 2d), with contour intervals of 0.5 m/s and 0.5 mm/day \bar{v}_{1000} and \bar{ppt} , respectively. Thickened contours denote the 0 m/s and 6 mm/day isolines. Shaded contours (with intervals of 0.02 m/s and 0.05 mm/day) denote regressions of the anomalies of each field onto the exchange time anomalies (i.e., the regressive estimates v_{1000}^* and ppt^* corresponding to a $+1\sigma$ deviation of τ').

1980s (Figure 3b). The CTM time series exhibits some significant secular trends, with convective intensity (Figure 3b, bottom curve) increasing and convective location drifting southward since the 1970s. (AGCM convective strength also has an upward trend, albeit weaker.) Such trends may be associated with the increase in tropical SSTs over the last few decades [Levitus *et al.*, 2000] and may reflect an increase in the intensity of the tropical circulation since the 1970s, as suggested by the tropical radiation budget analyses of Wielicki *et al.* [2002] and Chen *et al.* [2002].

[23] Both model frameworks are observed to show inconsistent phase relationships between IHT intensity and the interannual anomalies of *LOC* and *STR*. For instance, the sign of CTM-simulated IHT differs during the intense convective conditions of the early 1970s and late 1990s (fast IHT, blue shading) and the late 1980s (slow IHT, red shading). In light of the anomalies presented in Figure 2, however, discrepancies between annual mean IHT and convective variability are perhaps not unexpected. That is, the seasonality of the anomalous convection patterns described in section 3.2, e.g., reversals in the sense of the

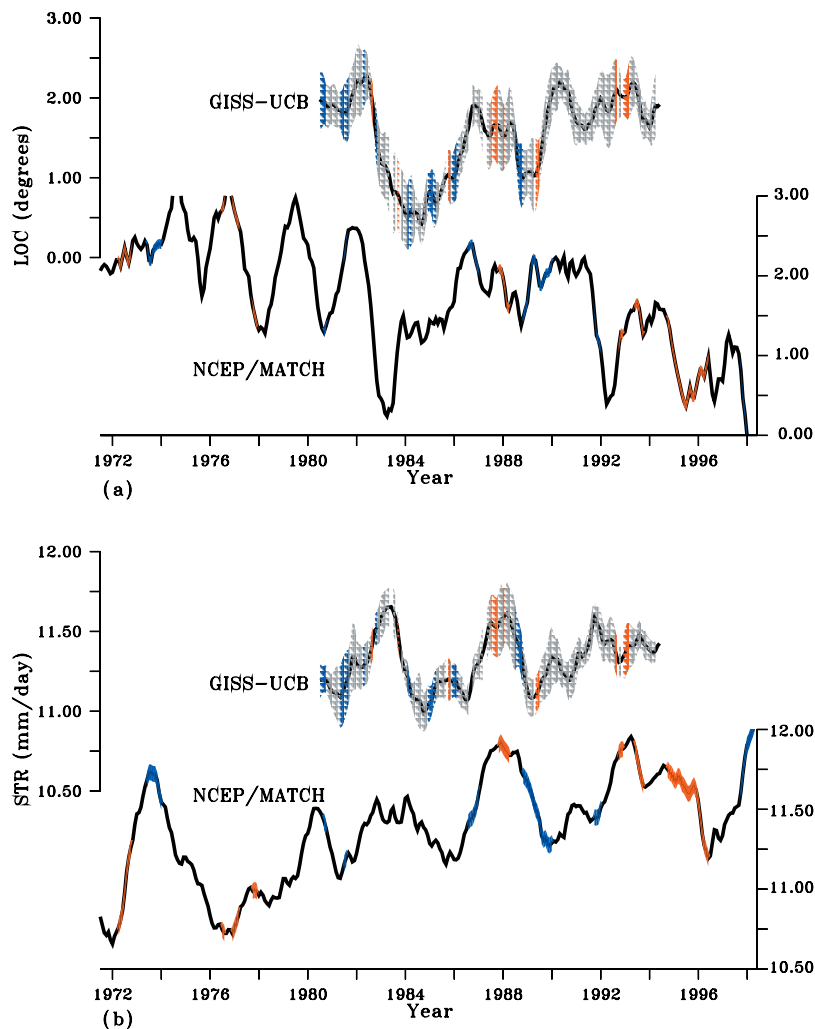


Figure 3. Interannual variations of convective displacement (LOC) and intensity (STR), (a) AGCM and (b) CTM. The anomalies are 12-point running means of deseasonalized, zonally averaged LOC and STR , and the error envelope in Figure 3a denotes the standard deviation of the ensemble mean. Blue (red) shading represents fast (slow) IHT conditions.

“anomalous convective dipole” between the winter and summer seasons, may obfuscate the influences of convective variability on IHT.

[24] Because the interannual time series of LOC and STR are relatively noisy with respect to fast and slow IHT conditions, a more sophisticated approach is required to elucidate the relationship between interhemispheric tracer transport and convective displacement and intensity variations. Thus monthly composites of LOC (Figure 4) and STR (Figure 5) have been computed over each longitudinal interval in Table 1 for those years with $\tau' \geq \sigma$ (red) and with $\tau' \leq -\sigma$ (blue). Separate fast and slow IHT composites are computed for both the AGCM and CTM simulations.

[25] Within the AGCM framework the zonally averaged fast and slow IHT convective displacement phase averages, $LOC_{\tau' \leq -\sigma}$ and $LOC_{\tau' \geq \sigma}$ (Figure 4a), are clearly separated by $\sim 3^\circ$ latitude in DJF and, to a lesser extent, by $\sim 1.5^\circ$ latitude in JJA. In contrast to zonally averaged LOC , both phases of zonally averaged STR have similar seasonal cycles, so that $STR_{\tau' \leq -\sigma}$ and $STR_{\tau' \geq \sigma}$ (Figure 5a) are not clearly

separated from one another, although there is a tendency for slow IHT conditions to be associated with lower precipitation rates (weaker convection), especially in JJA. Similar plots for the CTM qualitatively corroborate the AGCM results for zonally averaged convective displacement (Figure 4i), although the separation between fast and slow IHT phases is less pronounced, most likely because of the small sample size of the CTM data set (28 years) relative to the AGCM (75 years). Compared to the AGCM results, and despite the relatively large standard deviations, the zonally averaged STR phase averages for the CTM (Figure 5i) point to a greater role for anomalous ITCZ intensification as modulator of IHT interannual variability, especially during April–July when a clear separation of STR phases is evident.

[26] Many features of the zonally averaged statistics appear to be largely attributable to regional variations of ITCZ convective displacement and intensity. Over the Central Pacific and South America (Figures 4e and 4g), for example, the DJF ITCZ is displaced northward (southward) from its climatological location in years with anom-

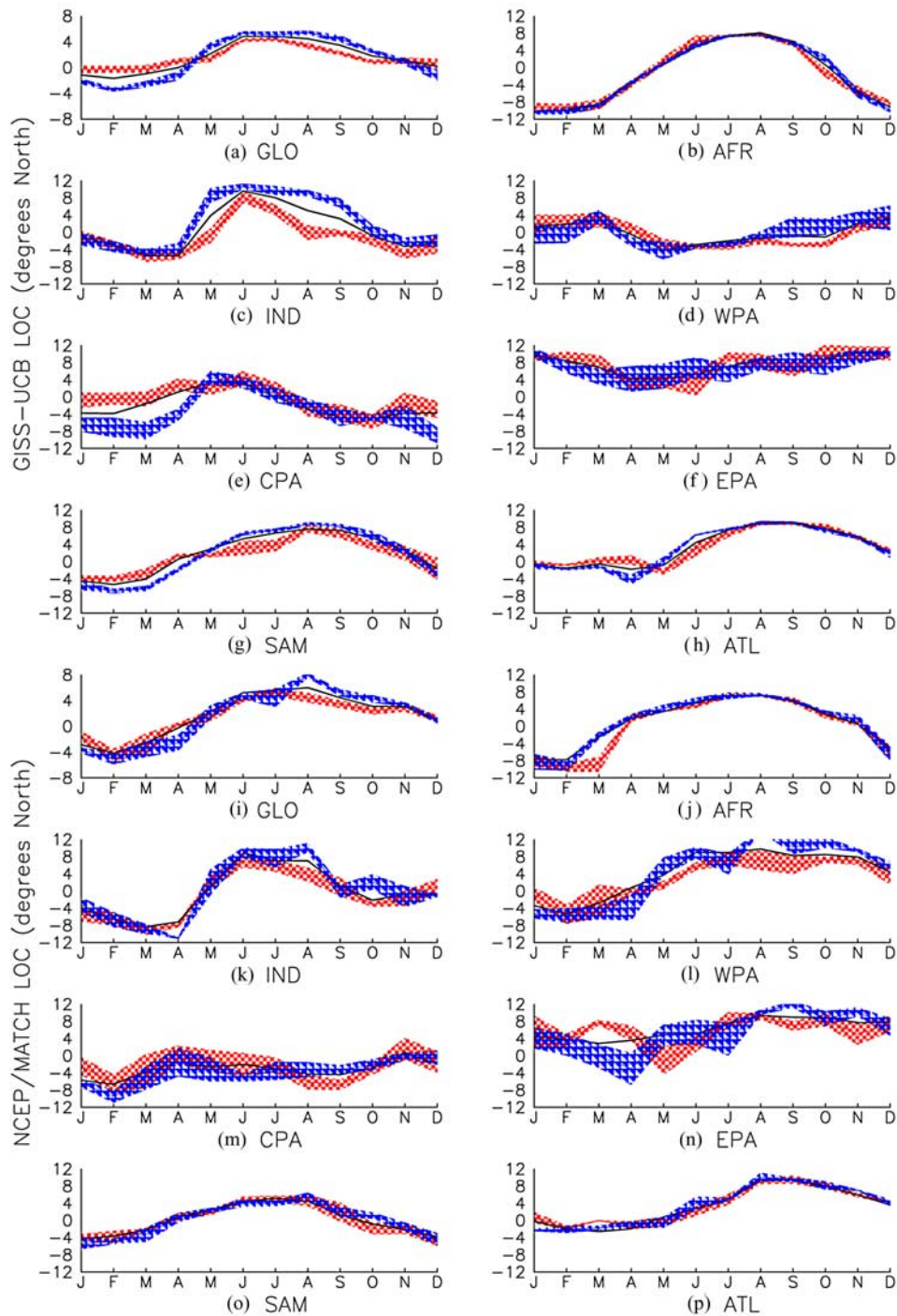


Figure 4. Composites of convective displacement (*LOC*) computed with respect to fast and slow IHT phases, (a) AGCM and (b) CTM. Blue (red) shading represents the composites for fast (slow) IHT conditions. The black line corresponds to the mean seasonal cycle of *LOC* computed over 1980–1994 (AGCM) or 1971–1998 (CTM). The regions illustrated in Figures 4a–4p are defined in Table 1.

alously slow (fast) IHT. During JJA anomalous displacements of similar magnitude are noted, mostly over the Indian Ocean region (Figure 4c). However, in contrast to the behavior during DJF, northward displacements of the Indian Ocean ITCZ during JJA are associated with anomalously fast IHT. These fast and slow IHT phased-averaged

Indian Ocean ITCZ displacements are especially well separated (by 6° – 8° degrees latitude) around the beginning (May) and end (August–September) of the southwest Indian Ocean Monsoon (IOM) active period. At this time of year, anomalous northward displacements of the ITCZ appear to be associated with strengthening of the cross-equatorial

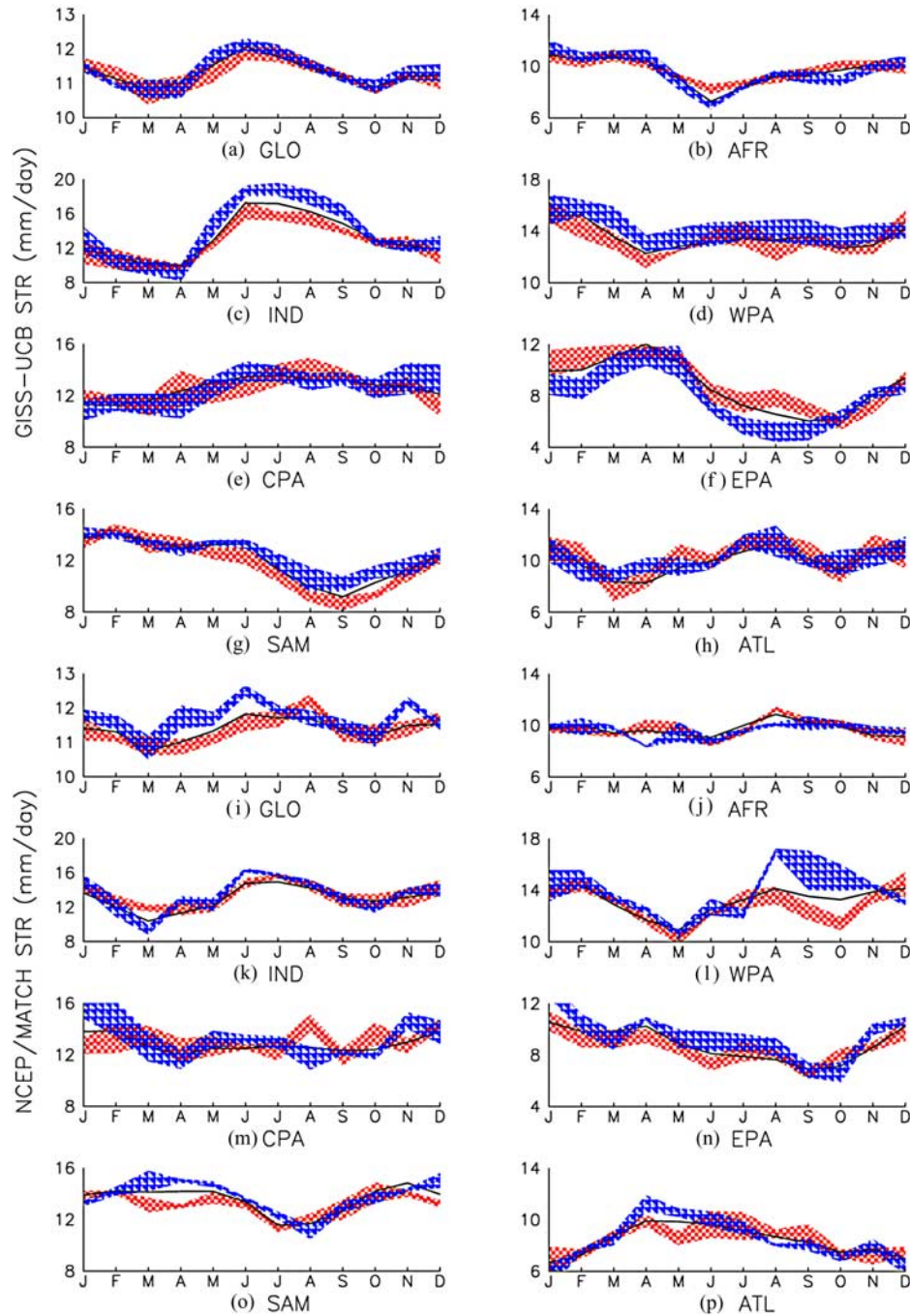


Figure 5. As in Figure 4, but for convective intensity (STR).

IOM circulation and enhanced interhemispheric mixing [Lintner, 2003]. Separation of the regional averages of $STR_{\tau' \leq -\sigma}$ and $STR_{\tau' \geq \sigma}$ are arguably less pronounced than the separation of regional averages of $LOC_{\tau' \leq -\sigma}$ and $LOC_{\tau' \geq \sigma}$ in the AGCM, although the relative reduction of May–September convective intensity along Indian Ocean ITCZ between fast and slow IHT conditions, by $\sim 15\%$, is notable (Figure 5c). Interestingly, there is an inverse relationship between exchange time variability and STR in the eastern Pacific (Figure 5f): anomalously slow IHT is associated with enhanced precipitation in this region.

[27] Certain features of the regional-scale, fast and slow IHT phases of LOC and STR for the CTM are qualitatively consistent with the AGCM results. For example, the separation of fast and slow IHT LOC and STR phases in the Indian Ocean region supports the weak intensity/southward displacement/slow IHT relationship during Northern Hemisphere summer (Figures 4k and 5k). However, the phase separations of LOC and STR in the region are rather modest compared to the AGCM. Other regional scale features of the fast and slow IHT phase averages of LOC and STR differ markedly between the AGCM and CTM. The Western

Pacific region, for instance, has a more pronounced JJA separation of convective displacement and intensity phases (Figures 4l and 5l) in the CTM. Interestingly, the climatologies of ITCZ displacement in the western Pacific are rather dissimilar in the AGCM and CTM frameworks: maximum ITCZ displacements occur much further to the north, by some 10° latitude, during May–October in the CTM than in the AGCM. To the extent that the climatology impacts how important various regions are in terms of their influence on global IHT, such intermodel climatology differences may contribute to the disparities between the AGCM- and CTM-simulated IHT.

[28] Together, Figures 4 and 5 suggest that within the AGCM framework, anomalous northward (southward) ITCZ displacements during Northern Hemisphere winter (summer) and, to a lesser extent, anomalously weak convection in the vicinity of the ITCZ are associated with anomalously slow tracer IHT, in agreement with the results of Figure 2. By contrast, for the CTM, on the other hand, fast and slow IHT signals are evident (and of similar magnitude) in both LOC and STR . It should be noted that the above results are robust to the choice of convective proxy, i.e., similar results are obtained if vertical velocity is used instead of precipitation rate, but they do exhibit some sensitivity to the manner in which the LOC and STR indices are defined.

3.4. Relative Importance of Convective Displacement and Intensity Variations

[29] In order to quantify the relative influence of each mode of convective variability on IHT, exchange times are now composited with respect to anomalies of convective location (LOC') and convective strength (STR'). As in section 3.3, an analogous “ 1σ selection criterion” is employed: only exchange times occurring with LOC' or STR' of magnitude $\geq 1\sigma$ are used to construct the phase averages. Three-month seasonal and annual mean composite differences, $\Delta\tau_{LOC} = \tau_{LOC \geq \sigma} - \tau_{LOC \leq -\sigma}$ and $\Delta\tau_{STR} = \tau_{STR \geq \sigma} - \tau_{STR \leq -\sigma}$, normalized with respect to either seasonal or annual mean τ , are computed and presented in Figure 6. For the AGCM, normalized seasonal mean values of $\Delta\tau_{LOC}$ of order ± 6 – 8% are noted for DJF, JJA, and September–October–November (SON) for zonally averaged ITCZ displacement, while normalized values of $\Delta\tau_{STR}$ are smaller with larger uncertainties (Figure 6a), i.e., differences in the location of the ITCZ exert a more sizeable impact on τ' than differences in convective strength.

[30] In contrast to the AGCM results, normalized seasonal mean $\Delta\tau_{LOC}$ for zonally averaged ITCZ displacements in the CTM are lower (of order ± 2 – 3%), although similar seasonality is evident (Figure 6b). The magnitudes of seasonal mean $\Delta\tau_{STR}$ for the CTM tend to exceed the values of $\Delta\tau_{LOC}$, with an approximate 3–4% reduction of exchange time for strong convection relative to weak convection. Together these results support the notion that, in a zonally averaged sense, LOC is a more significant modulator of IHT than STR in the AGCM, while both LOC and STR are of equal importance in the CTM. Overall, the relative predominance of ITCZ displacement variability within the GISS-UCB framework is consistent with the analysis of Gilliland [1997] using a different model (i.e.,

CCM3). However, the differences between the GISS-UCB and NCEP/MATCH results show that in order to obtain accurate simulations of IHT interannual variability, all aspects of convective variability must be accurately represented in models.

[31] Regionally, the relationship of exchange time variability to either LOC' or STR' is not uniform. In many regions, however, the error bars greatly exceed the seasonal mean $\Delta\tau_{LOC}$ and $\Delta\tau_{STR}$, especially for the CTM. Within the AGCM, $\Delta\tau_{LOC}$ is largest for the Indian Ocean region in JJA ($\sim -10\%$) and for South America and the Central Pacific regions ($\sim +6\%$) in DJF. The largest negative values of $\Delta\tau_{STR}$ ($\sim -9\%$), corresponding to enhanced IHT with increased convection, occur in the Indian Ocean region in JJA and the South American region in SON. Also noteworthy is the tendency for positive values of $\Delta\tau_{STR}$, i.e., slow IHT associated with enhanced convective conditions, in the eastern Pacific. In this region anomalous intensification of convection is associated with El Niño conditions, which have been noted in Figure 1b as well as elsewhere to be associated with anomalously slow IHT. For the most part $\Delta\tau_{LOC}$ and $\Delta\tau_{STR}$ for the Atlantic Ocean and Africa are negligible.

4. Discussion and Conclusions

[32] The results presented in section 3 highlight influences of both convective intensity and displacement as modulators of IHT. While the latter mechanism appears to be more dominant in the ensemble of AGCM runs, intensity changes are likely to play some role, at least during certain years. In the CTM both convective displacement and intensity variations play a comparable role in modulating IHT.

4.1. Influence of Convective Displacement

[33] In what sense do anomalous ITCZ displacements influence interhemispheric mixing? The present analysis suggests that slow IHT is associated with northward displacement of the ITCZ in DJF and southward displacement in JJA. Such ITCZ displacement changes are consistent with configurational changes of the Hadley circulation, namely a contraction of the winter hemisphere cell and/or an expansion of the summer hemisphere cell. Since the Hadley circulation is a significant source of meridional mixing in the tropics, a contraction of the winter hemisphere Hadley cell, the component of the Hadley circulation that straddles the equator during the solstice seasons, may diminish the efficiency of intertropical mixing. That is, during slow IHT conditions, the contracted winter cell does not extend as far into the summer hemisphere.

[34] The association between variations in the configuration of the Hadley circulation and IHT broadly agrees with the mechanism for modulating IHT proposed by Bowman and Cohen [1997]. Using a simple “two-mode” model of the Hadley circulation, Bowman and Cohen [1997] demonstrated that the degree of mixing between Hadley cells is controlled, in large part, by the relative amplitudes of the seasonal (nonstationary) mode of the Hadley circulation and the annual mean (stationary) mode. An increase in the seasonality of the Hadley circulation, which corresponds to more extreme meridional excursions of the ITCZ,

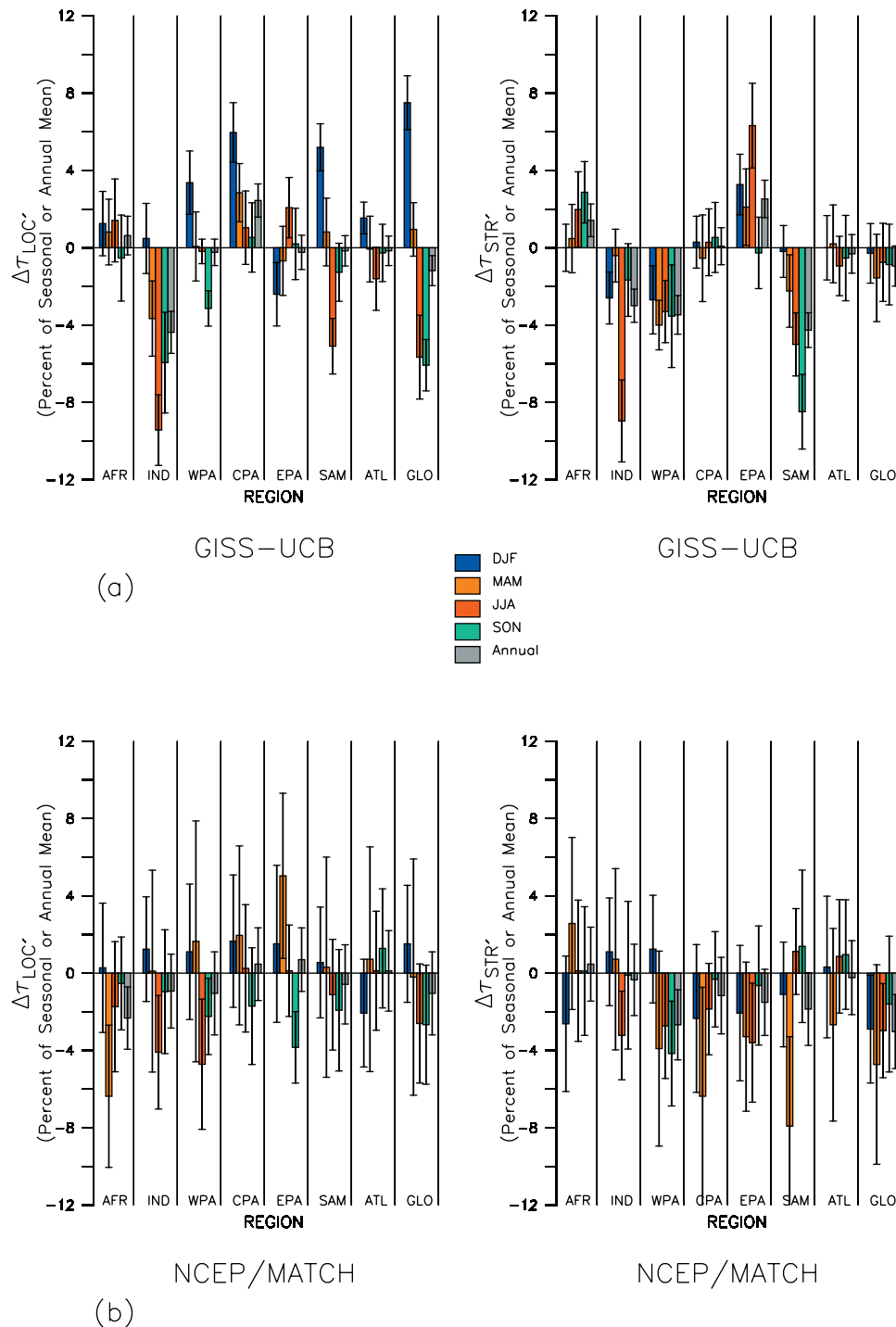


Figure 6. Seasonal and annual mean composite differences of exchange time computed with respect to LOC' and STR' , (a) AGCM and (b) CTM. The composite differences are normalized as percent relative to either the seasonal or annual mean. Error bars represent either a seasonal or annual mean aggregate of positive and negative phase standard deviations.

strengthens the interhemispheric mixing. The actual mechanism for increased mixing within the *Bowman and Cohen* [1997] model lies in the chaotic advective dispersion of air masses across streamlines: Increased seasonality produces more chaotic dispersion in the vicinity of the cell separatrix (the model “ITCZ”) resulting in greater exchange of air masses between the cells.

[35] Although it is not straightforward to ascertain the extent to which dispersion across streamlines may change in the models analyzed here, it is interesting that the relationship between exchange time variations and ITCZ displacements is similar whether the geodetic equator or the ITCZ (i.e., the dynamical equator) is selected as the interhemispheric partition (results not shown). That is, the collocation

of the hemispheric partition with the dynamical equator has very little impact on the relationship of anomalous IHT to anomalous ITCZ displacements. This result intimates that the anomalous ITCZ displacements do appear to bring about more vigorous intertropical mixing, consistent with the findings of *Bowman and Cohen* [1997]. In the absence of such displacement-induced mixing effects, the geodetic and dynamical partitionings of the hemispheres would likely produce more divergent exchange time interannual variations than are seen in the AGCM results.

[36] It should be noted that within the context of a two box model formulation, it is difficult to assess the extent to which the ITCZ displacements or changes in the Hadley circulation geometry may be associated with changes in interhemispheric mixing between the extratropics of one hemisphere and the other. That is, the two-box model formulation treats both hemispheres as uniformly well-mixed boxes. In reality, variations in the total timescale of interhemispheric mixing may be associated not only with variations of the timescale for intertropical mixing but also the timescale of extratropical-tropical mixing. An alternative formulation that may be better suited to addressing this aspect of interhemispheric mixing is a three-box model [*Bowman and Carrie*, 2002].

4.2. Influence of Convective Intensity

[37] The relatively weak influence of *STR* on IHT interannual variations in the AGCM is somewhat surprising. After all, convective intensity is thought to control the amount of upper level outflow of tracer mass, and both modeling and observational studies point to substantial fractions of climatological IHT occurring in the upper troposphere near regions of deep convection [*Hartley and Black*, 1995; *Staudt et al.*, 2001]. However, while convective intensification may produce more upper level outflow of air, enhanced vertical mixing also reduces vertical tracer gradients and lowers near-surface tracer concentrations. Thus variations in convective strength could hypothetically have an inverse relationship with respect to IHT if the vertical transport of tracer reduces the meridional transport in the lower troposphere. Here it should be noted that, if a tracer maintains a steep vertical gradient in the presence of enhanced vertical mixing, convective intensification may indeed produce more rapid IHT.

4.3. Zonally Averaged Versus Regional Influences

[38] Ultimately, the analysis of regional-scale convective variability suggests that the relationships between anomalous exchange time and regional *LOC'* and *STR'* should not be understated. The regional analysis points to some specific longitudinal intervals as centers of control of τ interannual variations, with some seasonal differences in terms of the regional control. For example, within the AGCM framework, convective variability in the central Pacific and South America appears to be an important modulator of IHT fluctuations in DJF. On the other hand, during JJA, the Indian Ocean ITCZ stands out as a center of control of IHT interannual variability, as both anomalous northward displacements and strengthening of convection along the Indian Ocean ITCZ are associated with reduced exchange times during Northern Hemisphere summer. Such changes appear to be associated with a strengthened IOM; a

more thorough treatment of the IOM influence on IHT will be provided in a separate study. Significantly, the regional controls of IHT variability may differ between the AGCM and CTM frameworks.

4.4. Differences Between the GISS-UCB and NCEP/MATCH Results

[39] An important finding of this study is that there are some substantial differences between the AGCM and CTM exchange times and their interannual variations. Direct comparison of the anomaly time series in Figure 1b shows only weak correspondence between the AGCM and CTM interannual variations with a correlation coefficient of only 0.17 over the 15-year period of overlap. Some of these differences may be attributable to dissimilarities in the features of the two model frameworks including the boundary layer and convective parameterization schemes utilized. Although the AGCM simulates realistic interannual variations in observables like temperature and precipitation, the simulation of tracer transport may be less realistic as it involves interactions between circulation and the spatial characteristics of the tracer field such as vertical gradients. Indeed, large intermodel discrepancies have been noted between vertical tracer profiles even when the horizontal distributions are more or less similar [*Denning et al.*, 1999].

[40] Within the specific context of the convective displacement and intensity mechanisms considered in this analysis, there is some agreement between the AGCM and CTM influences of the zonally averaged convection statistics: In both cases, more extreme meridional displacements of the zonally averaged ITCZ as well as enhanced ITCZ convection lead to stronger passive tracer IHT, although the relative importance of these mechanisms is not the same in each model. For the regional averages some sizeable discrepancies between the models have been documented, especially over the western Pacific. It is somewhat surprising that the influence of ENSO on IHT differs between the two model frameworks. However, the GISS-UCB AGCM and NCEP Reanalysis exhibit some differences in their patterns of ENSO-induced convective anomalies, especially over the western Pacific and Indian Ocean regions. Given the contributions to exchange time variations from localized convective influences, it is not unreasonable to expect some substantial model-to-model variation.

[41] **Acknowledgments.** The authors thank Roger Dargaville for use of the NCEP/MATCH fossil fuel run simulation, John Chiang, Ken Bowman, Ellen Cooter, Carey Jang, and two anonymous reviewers for valuable comments and discussions of the text, and Jasmin John for computational assistance. The United States Environmental Protection Agency through its Office of Research and Development collaborated in the research described here. It has been subjected to Agency review and approved for publication. Financial support for this work was provided by NSF grant ATM-9987457, NASA Carbon Program grant NAG5-11200, and NASA EOS-IDS grant NAG5-9514.

References

- Bowman, K. P., and G. D. Carrie (2002), The mean-meridional transport circulation of the troposphere in an idealized GCM, *J. Atmos. Sci.*, *59*, 1502–1514.
- Bowman, K. P., and P. J. Cohen (1997), Interhemispheric exchange by seasonal modulation of the Hadley circulation, *J. Atmos. Sci.*, *54*, 2045–2059.
- Chan, S. C., and J. L. Evans (2002), Comparison of the structure of the ITCZ in the West Pacific during the NH summers of 1989–1993 using AMIP simulations and ECMWF reanalysis, *J. Clim.*, *15*, 3549–3568.

- Chen, J., B. E. Carlson, and A. D. Del Genio (2002), Evidence for strengthening of the tropical general circulation in the 1990s, *Science*, *295*, 838–841.
- Chiang, J. C. H., Y. Kushnir, and S. E. Zebiak (2000), Interdecadal changes in eastern Pacific ITCZ variability and its influence on the Atlantic ITCZ, *Geophys. Res. Lett.*, *27*, 3687–3690.
- Cunnold, D. M., P. J. Fraser, R. F. Weiss, R. G. Prinn, P. G. Simmonds, B. R. Miller, F. N. Alyea, and A. J. Crawford (1994), Global trends and annual releases of CCl₃F and CCl₂F₂ from ALE/GAGE and other measurements from July 1978 to June 1991, *J. Geophys. Res.*, *99*, 1107–1126.
- Dargaville, R. J., S. C. Doney, and I. Y. Fung (2003), Interannual variability in the interhemispheric atmospheric CO₂ gradient: contributions from transport and the seasonal rectifier, *Tellus, Ser. B*, *55*, 711–722.
- Del Genio, A. D., and M. S. Yao (1988), Sensitivity of a global climate model to the specification of convective updraft and downdraft mass fluxes, *J. Atmos. Sci.*, *45*, 293–318.
- Del Genio, A. D., and M. S. Yao (1993), Efficient cumulus parameterization for long-term climate studies: The GISS scheme, in *The Representation of Cumulus Convection in Numerical Models*, edited by K. A. Emanuel and D. A. Raymond, *Meteorol. Monogr.*, *24*(46), 181–184.
- Denning, A. S., et al. (1999), Three-dimensional transport and concentration of SF₆—A model intercomparison study (TransCom 2), *Tellus, Ser. B*, *51*, 266–297.
- Dima, I. M., and J. M. Wallace (2003), On the seasonality of the Hadley cell, *J. Atmos. Sci.*, *60*, 1522–1527.
- Dlugokencky, E. J., L. P. Steele, P. M. Lang, and K. A. Masarie (1994), The growth rate and distribution of atmospheric methane, *J. Geophys. Res.*, *99*, 17,021–17,043.
- Elkins, J. W., T. M. Thompson, T. H. Swanson, J. H. Butler, B. D. Hall, S. O. Cummings, D. A. Fisher, and A. G. Raffo (1993), Decrease in the growth rates of atmospheric chlorofluorocarbon-11 and chlorofluorocarbon-12, *Nature*, *364*, 780–783.
- Gates, W. L., et al. (1999), An overview of the results of the Atmospheric Model Intercomparison Project (AMIP I), *Bull. Am. Meteorol. Soc.*, *80*, 29–55.
- Giannini, A., J. C. H. Chiang, M. A. Cane, Y. Kushnir, and R. Seager (2001), The ENSO teleconnection to the tropical Atlantic Ocean: Contributions of the remote and local SSTs to rainfall variability in the tropical Americas, *J. Clim.*, *14*, 4530–4544.
- Gilliland, A. B. (1997), Potential influences of ENSO on interhemispheric transport, Ph.D. thesis, Ga. Inst. of Technol., Atlanta, Ga.
- Gilliland, A. B., and D. E. Hartley (1998), Interhemispheric transport and the role of convective parameterizations, *J. Geophys. Res.*, *103*, 2039–2045.
- Gurney, K. R., R. M. Law, A. S. Denning et al. (2003), TransCom3 CO₂ inversion intercomparison: 1. Annual-mean control results and sensitivity to transport and prior flux information, *Tellus, Ser. B*, *55*, 555–579.
- Hansen, J., et al. (1997), Forcings and chaos in interannual to decadal climate change, *J. Geophys. Res.*, *102*, 25,679–25,720.
- Hartley, D. E., and R. X. Black (1995), A mechanistic analysis of interhemispheric transport, *Geophys. Res. Lett.*, *22*, 2945–2948.
- Janicot, S. (1997), Impact of warm ENSO events on atmospheric circulation and convection over the tropical Atlantic and West Africa, *Ann. Geophys.*, *15*, 471–475.
- Kalnay, E., et al. (1996), The NMC/NCAR reanalysis project, *Bull. Am. Meteorol. Soc.*, *77*, 437–471.
- Levin, I., and V. Heshaimer (1996), Refining of atmospheric transport model entries by the globally observed passive tracer distribution of krypton-85 and sulfur hexafluoride (SF₆), *J. Geophys. Res.*, *101*, 16,745–16,755.
- Levitus, S., J. I. Antonov, T. P. Boyer, and C. Stephens (2000), Warming of the world ocean, *Science*, *287*, 2225–2229.
- Lintner, B. R. (2003), Mechanisms of passive tracer interhemispheric transport: An analysis of model-derived and observational interhemispheric transport climatology and interannual variations, Ph.D. thesis, 264 pp., Univ. of Calif., Berkeley.
- Mahowald, N. M., P. J. Rasch, B. E. Eaton, S. Whittlestone, and R. G. Prinn (1997), Transport of ²²²Rn to the remote troposphere using the Model of Atmospheric Transport and Chemistry and assimilated winds from ECMWF and the National Center For Environmental Prediction/NCAR, *J. Geophys. Res.*, *102*, 28,139–28,151.
- Oort, A. H., and J. J. Yienger (1996), Observed interannual variability in the Hadley circulation and its connection to ENSO, *J. Clim.*, *9*, 2751–2767.
- Plumb, R. A., and J. D. Mahlman (1987), The zonally averaged transport characteristics of the GFDL general circulation/transport model, *J. Atmos. Sci.*, *44*, 298–327.
- Plumb, R. A., and D. D. McConlogue (1988), On the meridional structure of long-lived tropospheric constituents, *J. Geophys. Res.*, *93*, 15,897–15,913.
- Prather, M., M. McElroy, S. Wofsy, G. Russell, and D. Rind (1987), Chemistry of the global troposphere-fluorocarbons as tracers of air motion, *J. Geophys. Res.*, *92*, 6579–6613.
- Prinn, R., et al. (1992), Global average concentration and trend for hydroxyl radicals deduced from ALE/GAGE trichloroethane (methyl chloroform) data for 1978–1990, *J. Geophys. Res.*, *97*, 2445–2461.
- Prinn, R., R. F. Weiss, B. R. Miller, J. Huang, F. N. Alyea, D. M. Cunnold, P. J. Fraser, D. E. Hartley, and P. G. Simmonds (1995), Atmospheric trends and lifetime of CH₃CCl₃ and global OH concentrations, *Science*, *269*, 187–192.
- Rasch, P. J., and M. G. Lawrence (1998), Recent developments in transport methods at NCAR, in MPI Workshop on Conservative Transport Methods, edited by B. Machenhauer, *Rep. 265*, Max Planck Inst. for Meteorol., Hamburg, Germany.
- Rasch, P. J., N. M. Mahowald, and B. E. Eaton (1997), Representations of transport, convection, and the hydrologic cycle in chemical transport models: Implications of the modeling of short-lived and soluble species, *J. Geophys. Res.*, *102*, 28,127–28,138.
- Rind, D., and J. Lerner (1996), Use of on-line tracers as a diagnostic tool in general circulation model development: 1. Horizontal and vertical transport in the troposphere, *J. Geophys. Res.*, *101*, 12,667–12,683.
- Rind, D., J. Lerner, and C. McLinden (2001), Changes of tracer distributions in the doubled CO₂ climate, *J. Geophys. Res.*, *106*, 28,061–28,079.
- Russell, G. L., and J. A. Lerner (1981), A new finite-differencing scheme for the tracer transport equation, *J. Appl. Meteorol.*, *20*, 1483–1498.
- Staudt, A. C., D. J. Jacob, J. A. Logan, D. Bachiocchi, T. N. Krishnamurti, and G. W. Sachse (2001), Continental sources, transoceanic transport, and interhemispheric exchange of carbon monoxide over the Pacific, *J. Geophys. Res.*, *106*, 32,571–32,590.
- Steele, L. P., E. J. Dlugokencky, P. M. Lang, P. P. Tans, R. C. Martin, and K. A. Masarie (1992), Slowing down of the global atmospheric accumulation of methane during the 1980s, *Nature*, *358*, 313–316.
- Vuille, M., R. S. Bradley, M. Werner, R. Healy, and F. Keimig (2003), Modeling δ¹⁸O in precipitation over the tropical Americas: 1. Interannual variability and climatic controls, *J. Geophys. Res.*, *108*(D6), 4174, doi:10.1029/2001JD002038.
- Waliser, D. E., and C. Gautier (1993), A satellite derived climatology of the ITCZ, *J. Clim.*, *6*, 2162–2174.
- Wang, K. Y., and D. E. Shallcross (2000), A modeling study of tropospheric distributions of the trace gases CFC13 and CH₃CCl₃ in the 1980s, *Ann. Geophys.*, *18*, 972–986.
- Wielicki, B. A., et al. (2002), Evidence for large decadal variability in the tropical mean radiative energy budget, *Science*, *295*, 841–844.

I. Y. Fung, Berkeley Atmospheric Sciences Center and Department of Earth and Planetary Sciences, University of California, Berkeley, CA 94720, USA.

A. B. Gilliland, Office of Research and Development, NERL/AMD/MEARB, U.S. EPA, Mail Drop E243-01, Research Triangle Park, NC 27711, USA.

B. R. Lintner, Department of Geography, University of California, 507 McCone Hall, Berkeley, CA 94720, USA. (ben@atmos.berkeley.edu)